

## Some stereoisomers and tautomers of gemcitabine – A DFT treatment

Lemi Türker

Department of Chemistry, Middle East Technical University, Üniversiteler, Eskişehir Yolu No: 1, 06800 Çankaya/Ankara, Turkey  
e-mail: lturker@gmail.com; lturker@metu.edu.tr

### Abstract

Gemcitabine which is a cancer chemotherapy agent has a wide application against various types of tumors. In the present study, gemcitabine and its various stereoisomers and also its 1,3- and 1,5-type proton tautomers have been investigated within the constraints of density functional theory (DFT) at the level of B3LYP/6-311++G(d,p). All the isomers/tautomers presently considered (in vacuum conditions) have not only exothermic heat of formation values but also possess favorable Gibbs free energy of formation values and they are electronically stable. Various quantum chemical data have been collected and discussed including UV-VIS spectra.

### 1. Introduction

Gemcitabine is an antineoplastic agent with clinical activity against a wide range of solid tumors such as ovarian carcinoma, small cell and non-small cell lung cancers, head and neck cancer, bladder cancer, breast cancer, and pancreatic cancer [1]. It is rapidly deaminated in blood to the inactive metabolite 2',2'-difluorodeoxyuridine and is rapidly excreted by the urine [2]. To increase its therapeutic levels, gemcitabine is administered at high doses (1000 mg/m<sup>2</sup>) which cause side effects (neutropenia, nausea, and so forth). Unfortunately, many cancers develop resistance against this drug, such as loss of transporters and kinases responsible for the first phosphorylation step [2]. Cisplatin (CDDP), etoposide (VP-16), and mitomycin C (MMC) are well-known anticancer agents that are also active against many of these types of cancer. Because of the low toxicity profile of gemcitabine and the differences in mechanism of cytotoxicity, combinations of these drugs with gemcitabine were studied in *vitro* and in *vivo* conditions [1].

Gemcitabine is a fluorinated nucleoside currently administered against a number of cancers. It consists of a cytosine base and a 2-deoxy-2,2-difluororibose sugar. The synthetic challenges associated with the introduction of the fluorine atoms, as well as with nucleobase introduction of 2,2-difluorinated sugars, combined with the requirement to have an efficient process suitable for large scale synthesis, have spurred significant activity towards the synthesis of gemcitabine exploring a wide variety of synthetic approaches [3].

The literature of gemcitabine comprises innumerable aspects of related research [4-22]. Therapeutic efficacy of gemcitabine, which is used for breast cancer treatment, is severely compromised due to its rapid plasma degradation. Its hydrophilic nature poses a challenge for both its efficient encapsulation into nanocarrier systems and its sustained release property.

Dual enzymatic reactions were introduced to fabricate programmed gemcitabine (GEM) nanovectors for targeted pancreatic cancer therapy [16]. The clinical performance of gemcitabine is severely restricted by its

unsatisfactory pharmacokinetic parameters and easy deactivation mainly because of its rapid deamination, deficiencies in deoxycytidine kinase (DCK), and alterations in nucleoside transporter. A large number of gemcitabine pro-drugs were synthesized by chemical modification of gemcitabine to improve its biostability and bioavailability [17].

The effect of gemcitabine is significantly weakened by its rapid plasma degradation. In addition, the systemic toxicity and drug resistance significantly reduce its chemotherapeutic efficacy. One of the recently developed approaches to improve conventional chemotherapy is based on the direct targeting of chemotherapeutics to cancer cells using the drug-peptide conjugates [18, 19].

Also mixed micelles was employed as a delivery system, to prevent rapid metabolic inactivation and narrow therapeutic window of gemcitabine, thus to improve the pharmacokinetic characteristics of it and enhance its antitumor efficacy [20].

A novel electrochemical sensor, based on a reduced graphene oxide (rGO) nanocomposite and a zirconium-based metal-organic framework (Zr-MOF) with terephthalic acid as a ligand was employed in order to identify gemcitabine, which is a chemotherapy drug that is commonly used to treat breast cancer [21].

In an other study, the molecular basis of combining photodynamic therapy (PDT), a light-triggered targeted anticancer therapy, with the traditional chemotherapeutic properties of the well-known cytotoxic agent gemcitabine has been reported [22].

Gemcitabine has a pyrimidinone structure, which can exist as a free base molecular form in crystals. It exhibits 1,3- and 15-type proton tautomerism. Tautomers are structural isomers of molecules, which in this case interconvert via proton transfer [23].

In the literature, some quantum chemical and spectral properties of gemcitabine has been investigated performing density functional (DFT) approach [24].

The present study deals with some stereoisomers and tautomers of gemcitabine within the constraints of a DFT treatment.

## 2. Method of Calculations

In the present study, all the initial optimizations of the structures leading to energy minima have been achieved first by using MM2 method which is then followed by semi empirical PM3 self consistent fields molecular orbital method [25-27]. Afterwards, the structure optimizations have been achieved within the framework of Hartree-Fock and finally by using density functional theory (DFT) at the level of B3LYP/6-311++G(d,p) [28,29]. Note that the exchange term of B3LYP consists of hybrid Hartree-Fock and local spin density (LSD) exchange functions with Becke's gradient correlation to LSD exchange [30]. The correlation term of B3LYP consists of the Vosko, Wilk, Nusair (VWN3) local correlation functional [31] and Lee, Yang, Parr (LYP) correlation correction functional [32]. In the present study, the normal mode analysis for each structure yielded no imaginary frequencies for the  $3N-6$  vibrational degrees of freedom, where  $N$  is the number of atoms in the system. This search has indicated that the structure of each molecule considered corresponds to at least a local minimum on the potential energy surface. Furthermore, all the bond lengths have been thoroughly searched in order to find out whether any bond cleavage occurred or not during the geometry optimization process. All these computations were performed by using SPARTAN 06 program [33].

### 3. Results and Discussion

Gemcitabine has three stereogenic centers in 2-deoxy-2,2-difluororibose moiety. Figure 1 shows numbering of gemcitabine backbone (and its stereoisomers) considered for the present treatment. The three stereogenic centers are coinciding with carbons C2, C4 and C5 according to the present numbering.

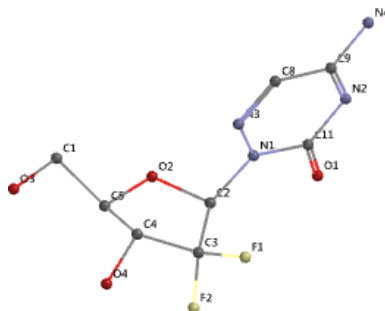


**Figure 1.** Numbering of gemcitabine backbone and its stereoisomers considered.

Optimized structures of the gemcitabine (I) and some of its stereo isomers considered are shown in Figure 2, together with types of the stereogenic centers they have. The figure also displays the direction of the dipole moment vectors and possible hydrogen bondings (dashed lines).

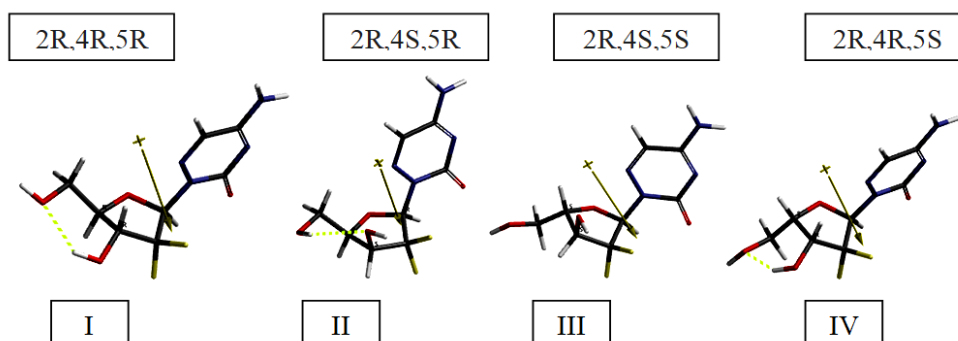


**Figure 2.** Optimized structures of the gemcitabine (I) and some of its stereo isomers considered. Hydrogen bonds are shown by dashed lines.

Table 1 shows some of the standard thermo chemical formation and constant volume heat capacity ( $C_v$ ) data of the species considered. The data reveal that the standard heat of formation ( $H^\circ$ ) values of all the isomers are exothermic and they are favored according to their  $G^\circ$  (Gibbs free energy of formation) values. The algebraic order of  $H^\circ$  and  $G^\circ$  values are I<IV<II<III and I<IV<III<II, respectively. The  $C_v$  data follow the order of I<IV<II<III.

**Table 1.** Some thermo chemical properties of the isomers considered.

Isomer	$H^\circ$	$S^\circ$ (J/mol $^\circ$ )	$G^\circ$	$C_v$ (J/mol $^\circ$ )
I	-2705634.209	490.73	-2705780.53	190.18
II	-2705630.271	485.58	-2705775.043	190.59
III	-2705629.195	491.59	-2705775.778	190.70
IV	-2705631.374	486.80	-2705776.513	190.47

Energies in kJ/mol.

Table 2 shows some energies of the species considered where E, ZPE and  $E_C$  stand for the total electronic energy, zero point vibrational energy and the corrected total electronic energy, respectively. According to the data, they are all electronically stable structures. The stability order is I> IV>II>III. Isomer-I is the most stable of all which possesses CH<sub>2</sub>OH and OH groups in such an orientation that in between a hydrogen bonding of 2.241 Å may happen although the distance is not very suitable. Thus some other factors might be operative. The hydrogen bond in isomer-II is in between -CH<sub>2</sub>OH and OH groups (-CH<sub>2</sub>OH---O), whereas in IV in between the same groups (H---OH) but hydrogen donor and acceptor are different in each case (see Figure 2). The hydrogen bonds are 2.303Å and 1.917Å, respectively. Thus, the hydrogen bond is stronger in IV compared to the one in isomer-II. Note that isomer-IV has OH possessing substituents (CH<sub>2</sub>OH and OH) in *endo,endo* whereas isomer-II in *exo,exo* stereochemistry.

**Table 2.** Some energies of the isomers considered.

Isomer	E	ZPE	$E_C$
I	-2706183.05	533.78	-2705649.27
II	-2706180.39	535.55	-2705644.84
III	-2706177.03	532.52	-2705644.51
IV	-2706181.11	535.03	-2705646.08

Energies in kJ/mol.

Aqueous and solvation energy values ( $E_{aq}$  and  $E_{solv}$ , respectively) for the isomers considered are shown in Table 3. The algebraic order of aqueous and solvation energy values are the same as IV<I<III<II. Orientation of the groups, thus their hydrogen bond formation possibilities and their stabilities, etc., dictate the orders obtained presently. The solvation energies were calculated by adopting SM5.4/A model [33].

**Table 3.** Some energies of the isomers considered.

Isomer	$E_{aq}$	$E_{solv}$
I	-2706292.68	-109.633
II	-2706284.46	-104.066
III	-2706284.64	-107.615
IV	-2706298.30	-117.193

Energies in kJ/mol. Solvation energy by SM5.4/A model.

Table 4 list some properties of the isomers considered. It is worth mentioning that the polar surface area (PSA) is defined as the amount of molecular surface area arising from polar atoms (N,O) together with their attached hydrogen atoms. Although these compounds are isomeric, their PSA values differ from each other, meaning that the same kind of atoms might be influenced by electronic factors differently at different positions.

**Table 4.** Some properties of the isomers considered.

Isomer	Area (Å <sup>2</sup> )	Volume (Å <sup>3</sup> )	PSA (Å <sup>2</sup> )	Ovality	Log P
I	242.29	212.36	99.100	1.41	-1.59
II	242.41	212.60	98.912	1.41	-1.59
III	243.82	212.84	101.454	1.41	-1.59
IV	239.22	211.91	96.969	1.39	-1.59

Polarizabilities in 10<sup>-30</sup> m<sup>3</sup> units.

As for the log P values, note that a negative value for log P means the compound has a higher affinity for the aqueous phase (it is more hydrophilic); when  $\log P = 0$  the compound is equally partitioned between the lipid and aqueous phases; whereas a positive value for log P denotes a higher concentration in the lipid phase (i.e., the compound is more lipophilic).

Figure 3 displays the chemical function descriptor (CFD) patterns of the isomers which are the present focus of interest.

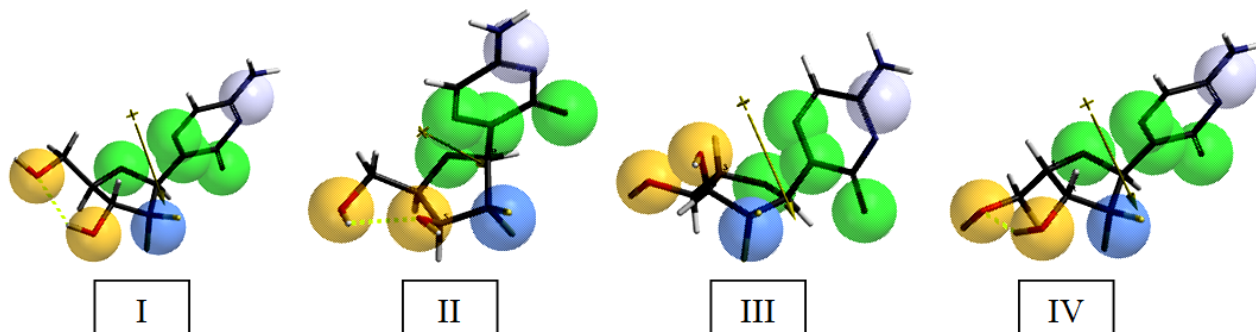


**Figure 3.** The CFD patterns of the isomers considered. (Yellow: HBD and HBA; Green: HBA; Blue: Hydrophobe; Purple: HBA, +ionizable).

As seen in the figure, all of the isomers possess the same hydrogen bond donor (HBD) and hydrogen bond acceptor (HBA) counts, namely 2 and 7, respectively. Each isomer has MW of 264.188 amu. So, all of them fulfill the criteria of Lipinsky rule (also known as Pfizer's rule of five) [34-36] and they all, like gemcitabine, should be in general orally active drugs. However, gemcitabine usually administered intravenously, mixed with other cancer chemotherapy agents [37]. Note that the rule of 5 (Lipinsky rule) states that poor absorption is more likely to occur when there are more than (i) five hydrogen-bond donors, (ii) ten hydrogen-bond acceptors, (iii) a molecular weight greater than 500, and (iv) a calculated Log P value greater than five.

The dipole moment and polarizability values for them are tabulated in Table 5. The orders of dipole moment and polarizability values are I>II>IV>III and III>II>I>IV, respectively. So, the stereochemistry of -CH<sub>2</sub>OH and -OH groups highly affects magnitude (as well as the direction) of the dipole moments. Note that the resultant dipole moment is the vectorial sum of bond dipoles.

**Table 5.** Dipole moment and polarizability values for the isomers considered.

Isomer	Stereochemistry at C4 and C5	Dipole moment	Polarizability
I	R,R	9.15	57.43
II	S,R	6.26	57.44
III	S,S	5.42	57.46
IV	R,S	5.75	57.39

Dipole moments in debye units. Polarizabilities in  $10^{-30}$  m<sup>3</sup> units. Refer Figures 1 and 2.

Figure 4 shows the electrostatic potential (ESP) charges on the atoms of the isomers considered. Their electrostatic potential maps are displayed in Figure 5 where negative potential regions reside on red/reddish and

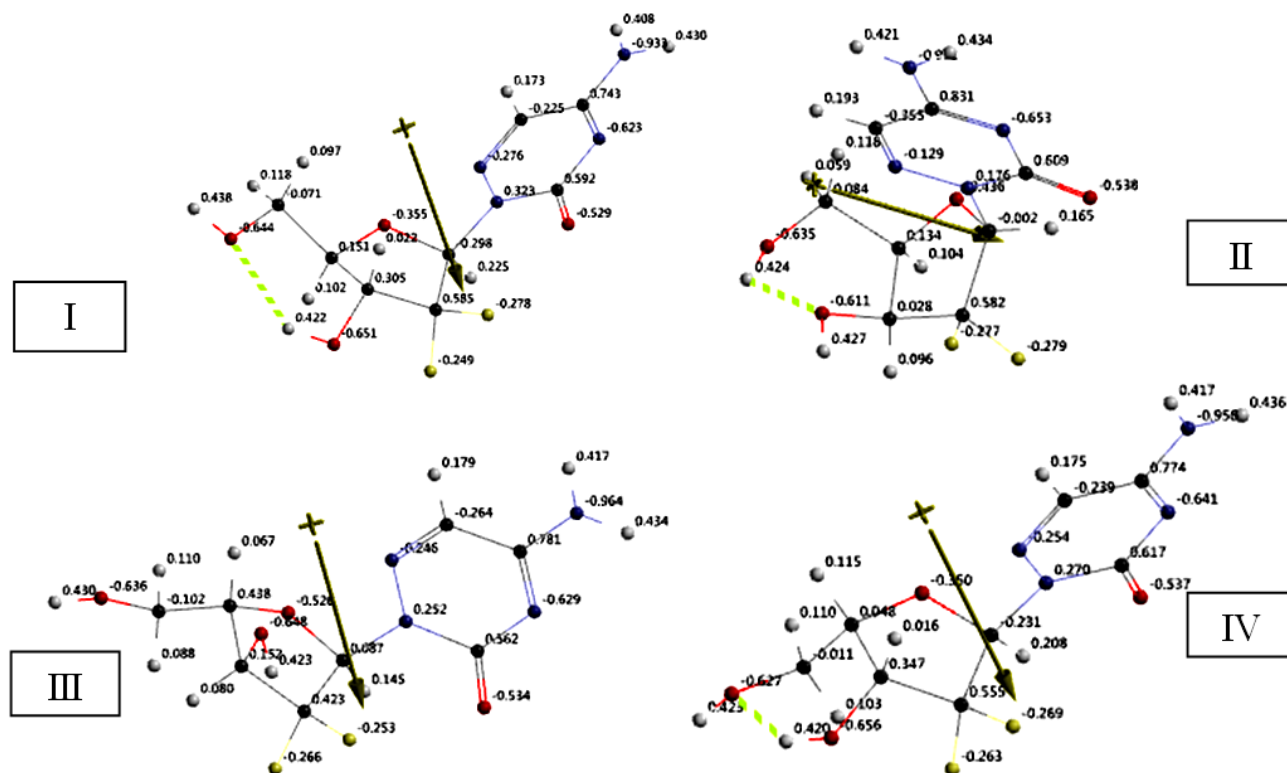


Figure 4. ESP charges on atoms of the isomers considered.

positive ones on blue/bluish parts of the maps. Note that the ESP charges are obtained by the program based on a numerical method that generates charges that reproduce the electrostatic potential field from the entire wavefunction [33]. Note that the stereo chemical changes greatly affect the locations of the positive and negative potential regions over the five-membered ring (also charge distribution, see Figure 4).

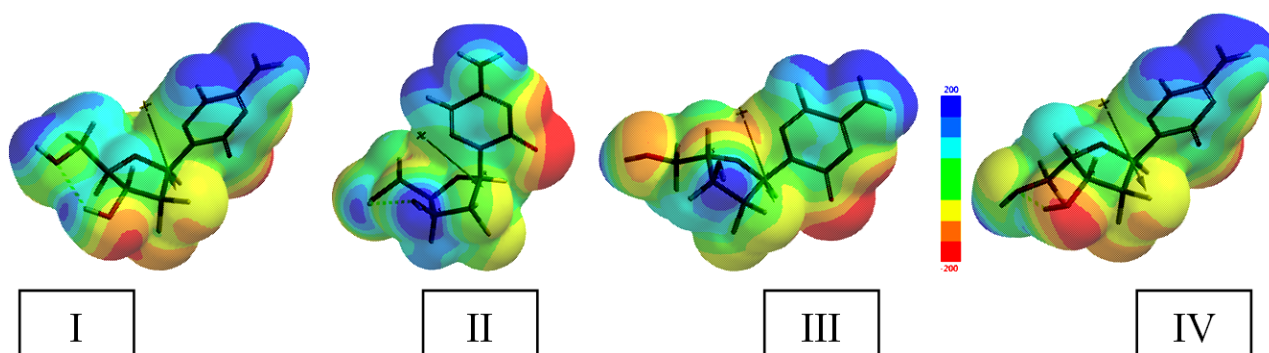
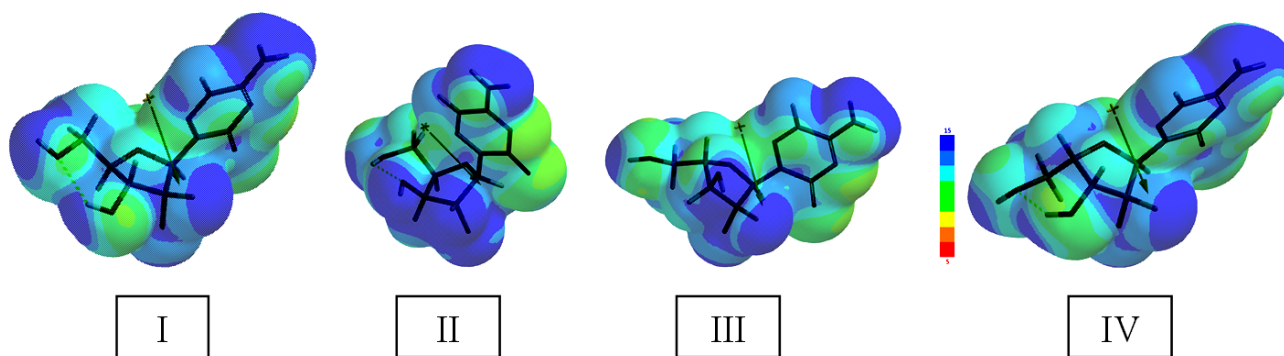


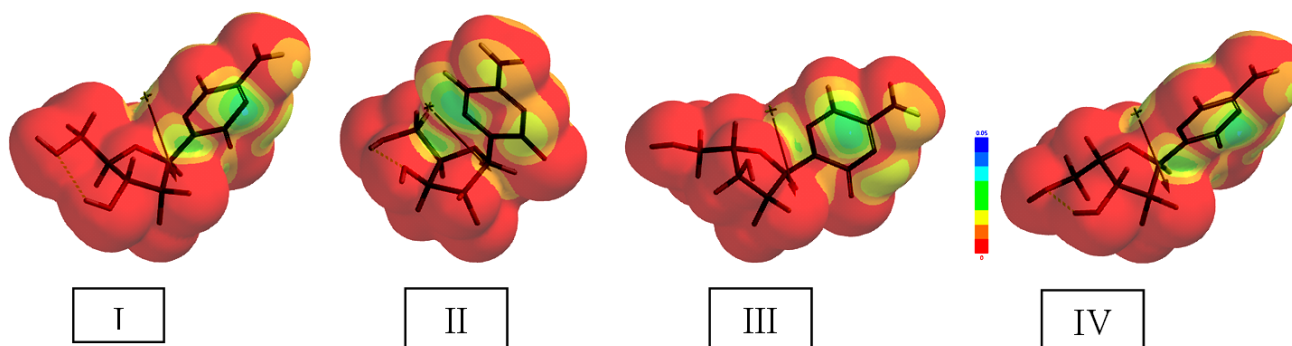
Figure 5. Electrostatic potential maps of the isomers considered.

Figure 6 shows the local ionization potential maps of the isomers considered where conventionally red/reddish regions (if any exists) on the density surface indicate areas from which electron removal is relatively easy, meaning that they are subject to electrophilic attack. It is worth remembering that the local ionization potential map is a graph of the value of the local ionization potential on an isodensity surface corresponding to a van der Waals surface.



**Figure 6.** The local ionization potential maps of the isomers considered.

The LUMO maps of the isomers considered are displayed in Figure 7. Note that a LUMO map displays the absolute value of the LUMO on the electron density surface. The blue color (if any exists) stands for the maximum value of the LUMO and the red colored region, associates with the minimum value. Note that the LUMO and NEXTLUMO are the major orbitals directing the molecule towards of the attack of nucleophiles [33]. Positions where the greatest LUMO coefficient exists is the most vulnerable site in nucleophilic reactions.



**Figure 7.** The LUMO maps of the isomers considered.

Figure 8 shows the bond densities of the isomers considered.

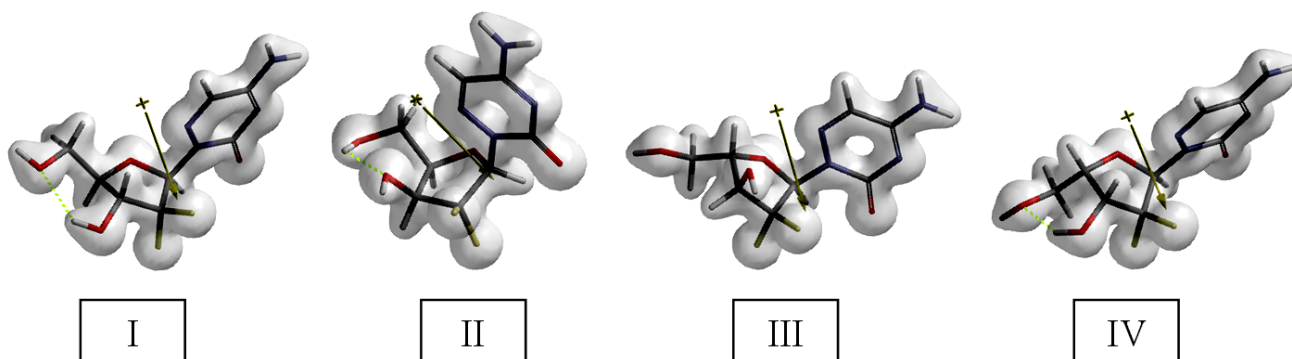


**Figure 8.** Bond densities of the isomers considered.

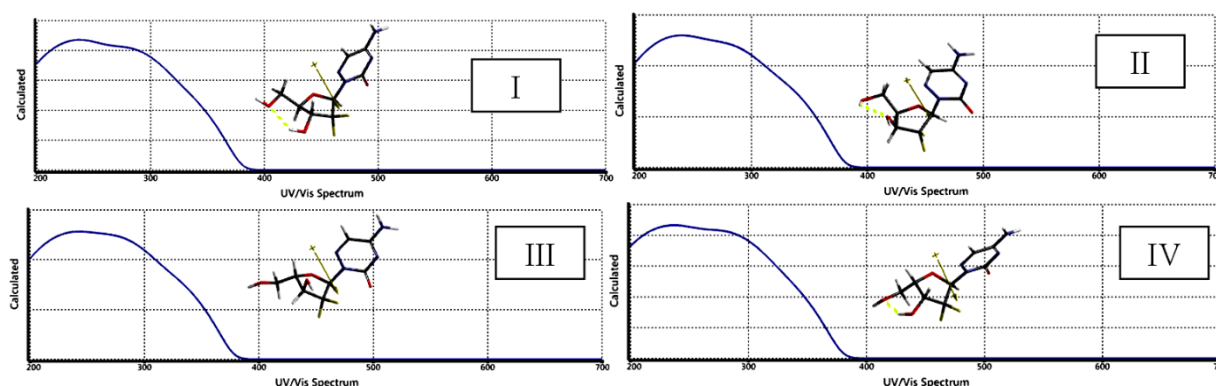
Table 6 lists the HOMO, LUMO energies and the interfrontier molecular orbital energy gap,  $\Delta\varepsilon$ , values ( $\Delta\varepsilon = \varepsilon_{\text{LUMO}} - \varepsilon_{\text{HOMO}}$ ) of the isomers considered. The algebraic orders of the HOMO and LUMO energies are I<IV<II<III and I<IV<III<II, respectively. Thus, the interfrontier molecular orbital energy gap values, constitute the order of III>II>I>IV.

**Table 6.** The HOMO, LUMO energies and  $\Delta\epsilon$  values of the isomers.

Isomer	HOMO	LUMO	$\Delta\epsilon$
I	-704.06	-226.62	477.44
II	-700.12	-220.53	479.59
III	-685.13	-202.68	482.45
IV	-702.76	-225.42	477.34

Energies in kJ/mol.

Figure 9 displays the calculated UV-VIS spectra (time dependent DFT) of the stereo isomers considered. As seen in the figure, all the spectra are confined into UV region only having some not well-developed shoulder, thus main peaks are broadened which do not vary much in shape for the isomers, so do the intensities and positions. The spectra and value of the transition moment which is responsible for the excitations of nonbonding or  $\pi$ -orbitals [38, 39] seem to be rather insensitive to molecular stereochemistry arising from the groups attached to the 5-membered ring. This statement is obvious because it has only  $\sigma$ -skeleton, lacking of any  $\pi$ -conjugation and through field effects seems to be very weak if any is operative.

**Figure 9.** The calculated UV-VIS spectra (TDDFT) of the isomers considered.

Gemcitabine (isomer-I) has two main proton tautomers; 1,3- and 1,5- tautomers (structures V and VI, respectively) which occur in the pyrimidone moiety of gemcitabine. Note that instances in chemistry are known that substances which are isomeric under certain given conditions are tautomeric under more drastic conditions [40].

Figure 10 shows the optimized structures of these tautomers. It also displays the direction of the dipole moment vectors. The tautomers V and VI have hydrogen bonding possibility having different lengths that is 2.264Å and 2.301Å, respectively.

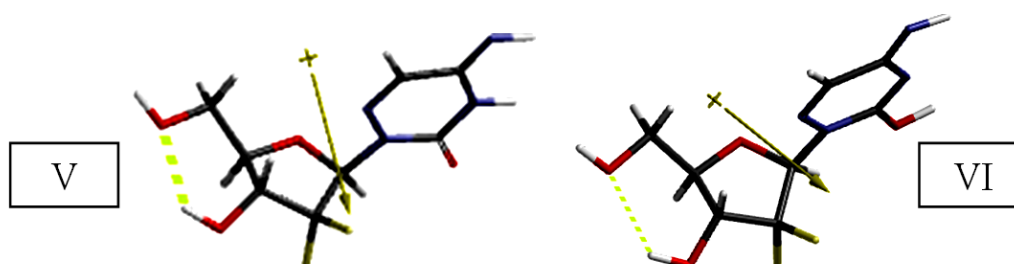
**Figure 10.** Optimized structures of the gemcitabine (I) tautomers considered.

Table 7 shows some thermo chemical properties of isomer-I and its tautomers V and VI. The data reveal that the tautomers have exothermic heat of formation ( $H^\circ$ ) and favorable  $G^\circ$  values as their parent gemcitabine (I). The 1,3-tautomer (V) is more exothermic and has more favorable standard Gibbs energy of formation values. The algebraic orders are  $I < V < VI$  for both  $H^\circ$  and  $G^\circ$  values of the species presented in Table 7. On the other hand,  $C_v$  values follow the order of  $I > VI > V$ .

**Table 7.** Some thermo chemical properties of isomer-I and its tautomers considered.

Isomer/tautomer	$H^\circ$	$S^\circ$ (J/mol $^\circ$ )	$G^\circ$	$C_v$ (J/mol $^\circ$ )
I	-2705634.209	490.73	-2705780.530	190.18
V	-2705622.158	482.26	-2705765.932	188.52
VI	-2705565.473	481.34	-2705708.984	188.56

Energies in kJ/mol.

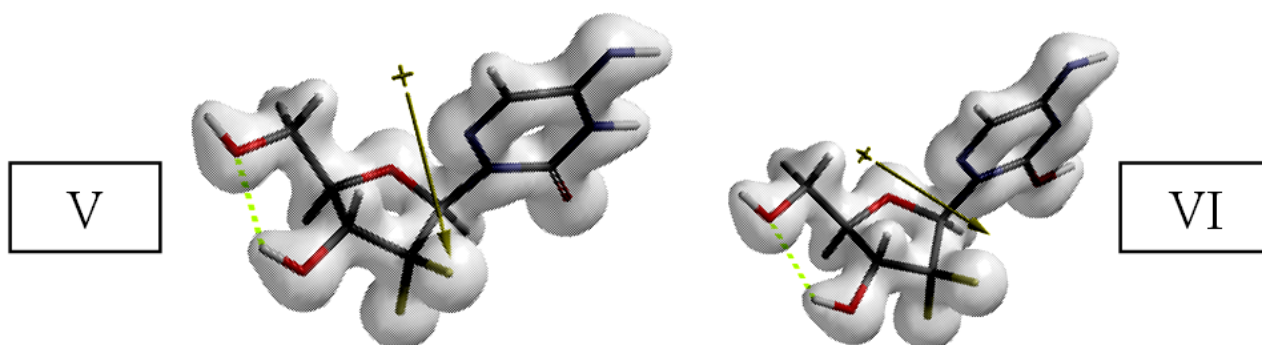
Some energies of isomer-I and its tautomers considered are shown in Table 8. The stability order of them is  $I > V > VI$ .

**Table 8.** Some energies of isomer-I and its tautomers considered.

Isomer/tautomer	E	ZPE	$E_C$
I	-2706183.05	533.78	-2705649.27
V	-2706172.70	536.59	-2705636.11
VI	-2706116.26	536.82	-2705579.44

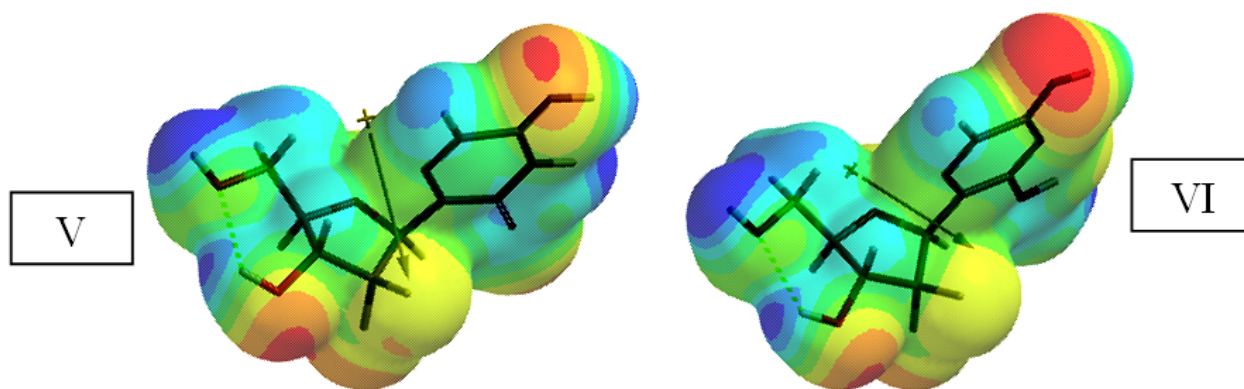
Energies in kJ/mol.

Figure 11 displays the bond densities of the gemcitabine (1) tautomers considered, namely structures V and VI.



**Figure 11.** Bond densities of the gemcitabine (1) tautomers considered.

Figure 12 is the electrostatic potential maps of the tautomers considered. Note that negative potential regions reside on red/reddish and positive ones on blue/bluish parts of the maps. Also note that structures V and VI stand for 1,3- and 1,5-proton tautomers, respectively. The 1,5-type tautomer possesses more extended conjugation than 1,3-tautomer. However, it is less favorable than the 1,3 -type. Note that thermal stability is mainly dictated by the inner-lying molecular orbitals [38,39].



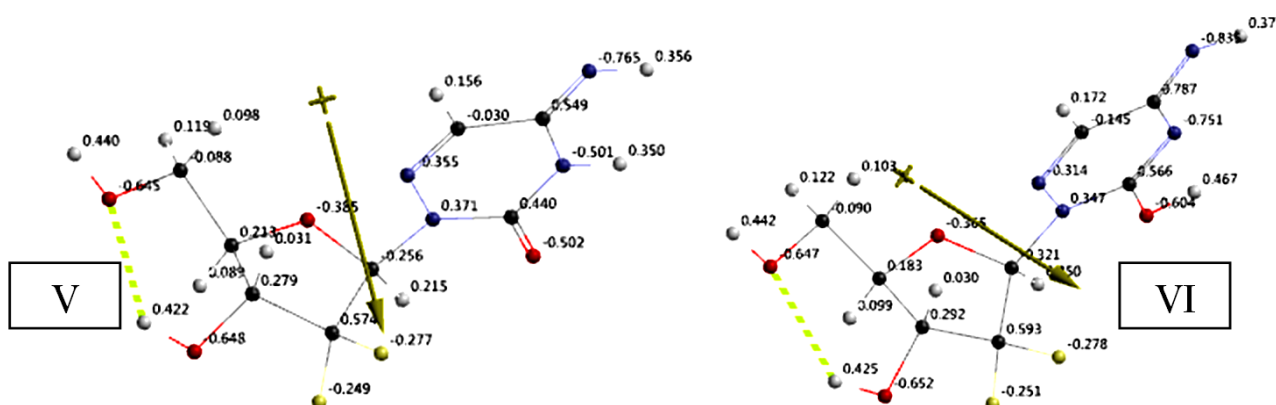
**Figure 12.** Electrostatic potential maps of the tautomers considered.

Table 9 lists some properties of the tautomers considered. As seen in the table tautomer-V has greater values than the respective ones for tautomer-VI, except the PSA and Log P values. It is interesting to be noted that the orders of PSA and  $C_v$  values of V and VI show parallelism (see Table 7). Also note that the opposite signs of the log P values of the tautomers V and VI which indicates the effect of tautomerism in these systems.

**Table 9.** Some properties of the tautomers considered.

Tautomers	Area ( $\text{\AA}^2$ )	Volume( $\text{\AA}^3$ )	PSA ( $\text{\AA}^2$ )	Ovality	Log P
V	242.56	212.69	99.201	1.41	-1.15
VI	241.81	212.34	100.091	1.40	0.16

The ESP charges on the atoms of the tautomers considered are shown in Figure 13.



**Figure 13.** The ESP charges on the atoms of the tautomers considered.

Table 10 tabulates the dipole moment and polarizability values for the tautomers considered.

**Table 10.** Dipole moment and polarizability values for the tautomers considered.

Tautomers	Dipole Moment	Polarizability
V	4.76	57.41
VI	3.83	57.41

Dipole moments in debye units. Polarizabilities in  $10^{-30} \text{ m}^3$  units.

Table 11 lists the HOMO, LUMO energies and  $\Delta\varepsilon$  values of isomer-I and its tautomers considered. The algebraic order of HOMO energies is  $V < I < VI$  whereas the LUMO energies possesses the order of  $I < V < VI$ . Thus, the interfrontier molecular orbital energy gap values,  $\Delta\varepsilon$ , have the order of  $V > VI > I$ . Thus, while proton migrates from amino moiety to the other position (nitrogen or oxygen) the interfrontier energy gap increases.

**Table 11.** The HOMO, LUMO energies and  $\Delta\varepsilon$  values of isomer-I and its tautomers (isomers).

Isomers	HOMO	LUMO	$\Delta\varepsilon$
I	-704.06	-226.62	477.44
V	-716.76	-218.93	497.83
VI	-667.23	-182.10	485.13

Energies in kJ/mol.

Figure 14 shows the calculated UV-VIS spectra (TDDFT) of the tautomers considered.

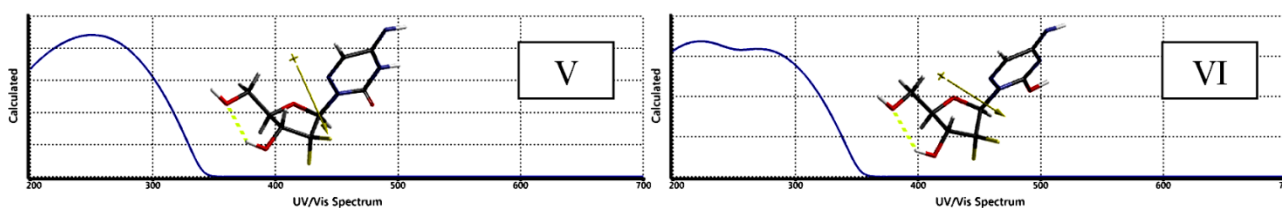


**Figure 14.** The calculated UV-VIS spectra (TDDFT) of the tautomers considered.

As seen in the figure, all the spectra are confined into UV region, but tautomer-VI has a shoulder, exhibiting some bathochromic effect, because it has more extended conjugation thus having narrower interfrontier molecular orbital energy gap compared to tautomer-V.

#### 4. Conclusion

In the present computational study, within the restrictions of DFT study at the level of B3LYP/6-311++G(d,p), various stereoisomers of gemcitabine and its 1,3- and 1,5-tautomers have been investigated. The present results indicate that in the vacuum conditions, all the structures are characterized with exothermic heat of formation and favorable Gibbs free energy of formation values and they are electronically stable. Some of the isomers and the tautomers considered may have hydrogen bonding possibility which affects the conformation of the substituents. Altogether with electronic effects the stereochemical and tautomeric variations result in varying outcomes on these systems. Thus, their potentials as chemotherapy agents, toxicological hazards etc., compared to the parent compound might be worth investigating.

#### References

- [1] van Moorsel, C.J., Veerman, G., Bergman, A.M., Guechev, A., Vermorken, J.B., Postmus, P.E., & Peters, G.J. (1997). Combination chemotherapy studies with gemcitabine. *Seminars in Oncology*, 24(2 Suppl 7), S7-17-S7-23. PMID: 9194475.
- [2] Moysan, E., Bastiat, G., & Benoit, J-P.(2013). Gemcitabine versus modified gemcitabine: A review of several promising chemical modifications. *Molecular Pharmaceutics. Mol. Pharmaceutics*, 10(2), 430-444. <https://doi.org/10.1021/mp300370t>

- [3] Brown, K., Dixey, M., Weymouth-Wilson, A., Linclau, B. (2014). The synthesis of gemcitabine. *Carbohydrate Research*, 387, 59-73. <https://doi.org/10.1016/j.carres.2014.01.024>
- [4] Chatzisisideri, T., Leonidis, G., Karamelas, T., Skavatsou, E., Velentza-Almpani, A., Bianchini, F., Tamvakopoulos, C., & Sarli, V. (2022). Integrin-mediated targeted cancer therapy using c(RGDyK)-based conjugates of gemcitabine. *Journal of Medicinal Chemistry*, 65 (1), 271-284. <https://doi.org/10.1021/acs.jmedchem.1c01468>
- [5] Zhong, H., Mu, J., Du, Y., Xu, Z., Xu, Y., Yu, N., Zhang, S., & Guo, S. (2020). Acid-triggered release of native gemcitabine conjugated in polyketal nanoparticles for enhanced anticancer therapy. *Biomacromolecules*, 21(2), 803-814. <https://doi.org/10.1021/acs.biomac.9b01493>
- [6] Jiang, Z., Pflug, K., Usama, S. M., Kuai, D., Yan, X., Sitcheran, R., & Burgess, K. (2019). Cyanine-gemcitabine conjugates as targeted theranostic agents for glioblastoma tumor cells. *Journal of Medicinal Chemistry*, 62(20), 9236-9245. <https://doi.org/10.1021/acs.jmedchem.9b01147>
- [7] Tam, Y.T., Huang, C., Poellmann, M., & Kwon, G.S. (2018). Stereocomplex prodrugs of oligo(lactic acid)-gemcitabine in poly(ethylene glycol)-block-poly(d,l-lactic acid) micelles for improved physical stability and enhanced antitumor efficacy. *ACS Nano*, 12(7), 7406-7414. <https://doi.org/10.1021/acs.nano.8b04205>
- [8] Zhang, H., Sun, Z., Wang, K., Li, N., Chen, H., Tan, X., Li, L., He, Z., & Sun, J. (2018). Multifunctional tumor-targeting cathepsin b-sensitive gemcitabine prodrug covalently targets albumin in situ and improves cancer therapy. *Bioconjugate Chemistry*, 29(6), 1852-1858. <https://doi.org/10.1021/acs.bioconjchem.8b00223>
- [9] Karamelas, T., Skavatsou, E., Argyros, O., Fokas, D., & Tamvakopoulos, C. (2017). Gemcitabine based peptide conjugate with improved metabolic properties and dual mode of efficacy. *Molecular Pharmaceutics*, 14(3), 674-685. <https://doi.org/10.1021/acs.molpharmaceut.6b00961>
- [10] Karamelas, T., Argyros, O., Sayyad, N., Spyridaki, K., Pappas, C., Morgan, K., Kolios, G., Millar, R.P., Liapakis, G., Tzakos, A.G., Fokas, D., & Tamvakopoulos, C. (2014). GnRH-gemcitabine conjugates for the treatment of androgen-independent prostate cancer: pharmacokinetic enhancements combined with targeted drug delivery. *Bioconjugate Chemistry*, 25(4), 813-823. <https://doi.org/10.1021/bc500081g>
- [11] Wang, S., Cen, D., & Zhang, C.A. (2024). Cathepsin B-sensitive gemcitabine prodrug for enhanced pancreatic cancer therapy. *Journal of Pharmaceutical Sciences*, 113(7), 1927-1933. <https://doi.org/10.1016/j.xphs.2024.03.018>
- [12] Wang, R., Li, Y., Gao, J., & Luan, Y. (2022). WRQ-2, a gemcitabine prodrug, reverses gemcitabine resistance caused by hENT1 inhibition. *Drug Discoveries & Therapeutics*, 16(6), 286-292. <https://doi.org/10.5582/ddt.2022.01077>
- [13] Hamsici, S., Ekiz, M.S., Ciftci, G.C., Tekinay, A.B., & Guler, M.O. (2017). Gemcitabine Integrated Nano-Prodrug Carrier System. *Bioconjugate Chemistry*, 28(5), 1491-1498. <https://doi.org/10.1021/acs.bioconjchem.7b00155>
- [14] Wang, M., Qu, K., Zhao, P., Yin, X., Meng, Y., Herdewijn, P., Liu, C., Zhang, L., & Xia, X. (2023). Synthesis and anticancer evaluation of acetylated-lysine conjugated gemcitabine prodrugs. *RSC Medicinal Chemistry*, 14(8), 1572-1580. <https://doi.org/10.1039/D3MD00190C>
- [15] Li, Y., Liu, Y., Chen, Y., Wang, K., & Luan, Y. (2022). Design, synthesis and antitumor activity study of a gemcitabine prodrug conjugated with a HDAC6 inhibitor. *Bioorganic & Medicinal Chemistry Letters*, 72, 128881. <https://doi.org/10.1016/j.bmcl.2022.128881>
- [16] Han, H., Valdepérez, D., Jin, B., Yang, Q., Li, Z., Wu, Y., Pelaz, B., Parak, W.J., & Ji, J. (2017). Dual enzymatic reaction-assisted gemcitabine delivery systems for programmed pancreatic cancer therapy. *ACS Nano*, 11(2), 1281-1291. <https://doi.org/10.1021/acs.nano.6b05541>

- [17] Han, H., Li, S., Zhong, Y., Huang, Y., Wang, K., Jin, Q., Ji, J., & Yao, K. (2022). Emerging pro-drug and nano-drug strategies for gemcitabine-based cancer therapy. *Asian Journal of Pharmaceutical Sciences*, 17(1), 35-52. <https://doi.org/10.1016/j.ajps.2021.06.001>
- [18] Hawrylkiewicz, A., & Ptasińska, N. (2021). Gemcitabine peptide-based conjugates and their application in targeted tumor therapy. *Molecules*, 26(2), 364. <https://doi.org/10.3390/molecules26020364>
- [19] Zhong, W., Zhang, X., Duan, X., Liu, H., Fang, Y., Luo, M., Fang, Z., Miao, C., Lin, D., & Wu, J. (2022). Redox-responsive self-assembled polymeric nanoprodrug for delivery of gemcitabine in B-cell lymphoma therapy. *Acta Biomaterialia* 144, 67-80. <https://doi.org/10.1016/j.actbio.2022.03.035>
- [20] Wang, Y., Fan, W., Dai, X., Katragadda, U., McKinley, DeAngelo., Teng, Q., & Tan, C. (2014). Enhanced tumor delivery of gemcitabine via PEG-DSPE/TPGS mixed micelles. *Molecular Pharmaceutics*, 11(4), 1140-1150. <https://doi.org/10.1021/mp4005904>
- [21] Shi, Z., Han, L., & Dong, Y. (2024). Electrochemical sensor based on reduced graphene oxide paste electrode for detection of gemcitabine as a chemotherapy drug in breast cancer. *Alexandria Engineering Journal*, 102, 49-57. <https://doi.org/10.1016/j.aej.2024.05.116>
- [22] Abdelgawwad, A.M.A., Roca-Sanjuán, D., & Francés-Monerris, A. (2023). Electronic spectroscopy of gemcitabine and derivatives for possible dual-action photodynamic therapy applications. *The Journal of Chemical Physics*, 159 (22), 224106. <https://doi.org/10.1063/5.0170949>
- [23] Barrington, H., & Samokhvalov, A. (2023). Characterization of tautomeric forms of anti-cancer drug gemcitabine and their interconversion upon mechano-chemical treatment, using ATR-FTIR spectroscopy and complementary methods. *Journal of Pharmaceutical and Biomedical Analysis*, 226, 115243, <https://doi.org/10.1016/j.jpba.2023.115243>
- [24] Rezkallah, E., Ibrahim, A., Dahy, A.R., Hakiem, A.A. and Mahfouz, R. (2019). DFT and thermal decomposition studies on gemcitabine. *Zeitschrift für Physikalische Chemie*, 233(10), 1503-1527. <https://doi.org/10.1515/zpch-2018-1304>
- [25] Stewart, J.J.P. (1989). Optimization of parameters for semi-empirical methods I. *J. Comput. Chem.*, 10, 209-220. <https://doi.org/10.1002/jcc.540100208>
- [26] Stewart, J.J.P. (1989). Optimization of parameters for semi-empirical methods II. *J. Comput. Chem.*, 10, 221-264. <https://doi.org/10.1002/jcc.540100209>
- [27] Leach, A.R. (1997). *Molecular modeling*. Essex: Longman.
- [28] Kohn, W., & Sham, L.J. (1965). Self-consistent equations including exchange and correlation effects. *Phys. Rev.*, 140, 1133-1138. <https://doi.org/10.1103/PhysRev.140.A1133>
- [29] Parr, R.G., & Yang, W. (1989). *Density functional theory of atoms and molecules*. London: Oxford University Press.
- [30] Becke, A.D. (1988). Density-functional exchange-energy approximation with correct asymptotic behavior. *Phys.Rev. A*, 38, 3098-3100. <https://doi.org/10.1103/PhysRevA.38.3098>
- [31] Vosko, S.H., Wilk, L., & Nusair, M. (1980). Accurate spin-dependent electron liquid correlation energies for local spin density calculations: a critical analysis. *Can. J. Phys.*, 58, 1200-1211. <https://doi.org/10.1139/p80-159>
- [32] Lee, C., Yang, W., & Parr, R.G. (1988). Development of the Colle-Salvetti correlation energy formula into a functional of the electron density. *Phys. Rev. B*, 37, 785-789. <https://doi.org/10.1103/PhysRevB.37.785>
- [33] SPARTAN 06 (2006). Wavefunction Inc. Irvine CA, USA.

- 
- [34] Lipinski, C.A., Lombardo, F., Dominy, B.W., & Feeney, P.J. (2012). Experimental and computational approaches to estimate solubility and permeability in drug discovery and development settings. *Adv Drug Delivery Rev.*, 64, 4-17. <https://doi.org/10.1016/j.addr.2012.09.019>
- [35] Lipinski, C.A. (2004). Lead- and drug-like compounds: the rule-of-five revolution. *Drug Discovery Today*, 1, 337-341. <https://doi.org/10.1016/j.ddtec.2004.11.007>
- [36] Lipinski, C.A. (2016). Rule of five in 2015 and beyond: Target and ligand structural limitations, ligand chemistry structure and drug discovery project decisions. *Advanced Drug Delivery Reviews*, 101, 34-41. <https://doi.org/10.1016/j.addr.2016.04.029>
- [37] Barton-Burke, Margaret (1999). Gemcitabine: A pharmacologic and clinical overview. *Cancer Nursing*, 22(2), 176-183.
- [38] Fleming, I. (1976). *Frontier orbitals and organic reactions*. London: Wiley.
- [39] Turro, N.J. (1991). *Modern molecular photochemistry*. Sausalito: University Science Books.
- [40] Reutov, O. (1970). *Theoretical principles of organic chemistry*, Moscow: Mir Pub.

---

This is an open access article distributed under the terms of the Creative Commons Attribution License (<http://creativecommons.org/licenses/by/4.0/>), which permits unrestricted, use, distribution and reproduction in any medium, or format for any purpose, even commercially provided the work is properly cited.

---